Acta Crystallographica Section B
Structural Science
ISSN 0108-7681

Structure of pyrrhotite 5*C* (Fe_9S_{10})

Alexander Dean Elliot

CSIRO Minerals Down Under Flagship, CSIRO Process Science and Engineering, Parker CRC for Integrated Hydrometallurgy Solutions, PO Box 7229, Karawara, Western Australia 6152, Australia

Correspondence e-mail: alexander.elliot@csiro.au

Received 31 August 2009
Accepted 29 March 2010

The distribution of vacancies throughout the underlying NiAs structure of pyrrhotite 5*C* was analysed through the application of vacancy avoidance and the closeness condition in conjunction with order–disorder layering. Two crystallographically equivalent structure solutions (chiral enantiomers) were produced consisting of layers containing one vacancy in every eight iron sites broken by a fully occupied layer every fifth iron layer, and best described by monoclinic statistical models. The statistical 5*C* structures were verified using synchrotron powder diffraction data as well as published electron-diffraction patterns. An order–disorder structure description is proposed for the intermediate pyrrhotites of which pyrrhotite 5*C* is an end-member.

1. Introduction

Pyrrhotite ($Fe_{1-x}S$), described by Pierce & Buseck (1974) as '*geologically interesting, industrially important, and crystallographically complex*', was extensively studied in the 1970s and early 1980s to shed light on its complex phase relations, structures, and magnetic and electric properties (Tokonami *et al.*, 1972). Several stable low-temperature forms of pyrrhotite (2-, 4-, 5-, 6- and 11*C*) have been identified in nature, forms which contain a superstructure related to the NiAs-type structure which has hexagonal cell dimension *a* around 3.45 Å and *c* around 5.8 Å (Carpenter & Desborough, 1964; Morimoto *et al.*, 1970; Fleet & Macrae, 1969; Vorma, 1970). The stable forms contain a stoichiometric composition of $Fe_{n-1}S_n$ ($n > 8$), where structures are classified as the $(n/2)C$ type for even *n* and *nC* type for odd *n*. A supercell with *c* dimension *n*/2 and *n* times that of the NiAs-type unit cell is required to describe the distribution of iron vacancies within the unit cell for even and odd *n* (Morimoto *et al.*, 1970).

It was Bertaut (1953) who first confirmed that the pyrrhotite superstructure could be built from NiAs structure with iron layers normal to the *c* axis, and demonstrated that it contained an ordered sequence of vacancies. His proposed structure for monoclinic 4*C*-type pyrrhotite, based on maximum vacancy separation, contained ordered vacancies in alternate iron layers, *FAFDFBFC*, where *A*, *B*, *C* and *D* are spatially different configurations of two vacancies in eight positions and *F* represents a full layer of Fe atoms, as illustrated in Fig. 1. Bertaut's structure was later confirmed and refined by Tokonami *et al.* (1972), and subsequently converted to the conventional space group *C*2/*c* with further refinement by Powell *et al.* (2004). Van Landuyt & Amelinckx (1972) predicted the significant presence of defect structures including anti-phase boundaries, stacking faults and twin boundaries in the 4*C* structure, which Nakazawa *et al.* (1975) confirmed using high-resolution electron microscopy. The

structure of triolite (2*C*-type, FFFF) was determined by Bertaut (1956) and refined by Evans (1970). For the low-temperature pyrrhotites, triolite, which contains fully occupied iron sites with hexagonal space-group symmetry, is the upper end-member of the pyrrhotite group in terms of iron content while pyrrhotite 4*C* is the lower end-member.

Nakazawa & Morimoto (1971) proposed that pyrrhotite 6*C* consists of iron vacancies in every third iron layer (*e.g. FAFFBFFCFFDF*). However, Nakazawa and Morimoto's proposed 6*C* structure fails to describe the X-ray diffraction intensity for the 6*C* structure (Koto *et al.*, 1975). Koto *et al.* (1975) determined and refined the 6*C* structure as a statistical distribution of vacancies with every third iron layer full with half iron occupancies in-between ($FC_{\frac{1}{2}}C_{\frac{1}{2}}FB_{\frac{1}{2}}B_{\frac{1}{2}}FD_{\frac{1}{2}}D_{\frac{1}{2}}FA_{\frac{1}{2}}A_{\frac{1}{2}}F$). The 6*C* structure was recently revisited by de Villiers & Liles (2010) who slightly refined the structure determined by Koto *et al.* (1975), in addition to proposing a second alternative structure for consideration.

Corlett (1968) proposed a 5*C* superstructure by adding two filled iron layers to the 4*C* structure (*e.g. FAFBFCFDFF*) to produce a structure with accumulated full layers. Vaughan *et al.* (1971) proposed a structure for 5*C* which features maximum dispersion of full and vacancy (*A*, *B*, *C* and *D*) layers with an alternating sequence of one and two filled layers between vacancy layers (*e.g. FAFBFFCFDF*) as a best fit to observed X-ray, magnetic, composition and Mössbauer data for a mixed 4*C*–5*C* sample. Dódony & Pósfai (1990) confirmed that some 5*C* superstructures can be modelled using a *FAFBFFCFDF* stacking sequence using TEM diffraction patterns taken from two directions perpendicular to the hexagonal *c* axis. However, other 5*C* structures were fit best with half of some vacant sites randomly occupied. Recently de Villiers *et al.* (2009) proposed a structure for 5*C* based on single-crystal X-ray diffraction which features vacancies in every iron layer, and includes two iron layers containing two vacancies in eight positions, with the remaining eight layers each containing less that one vacancy in eight positions.

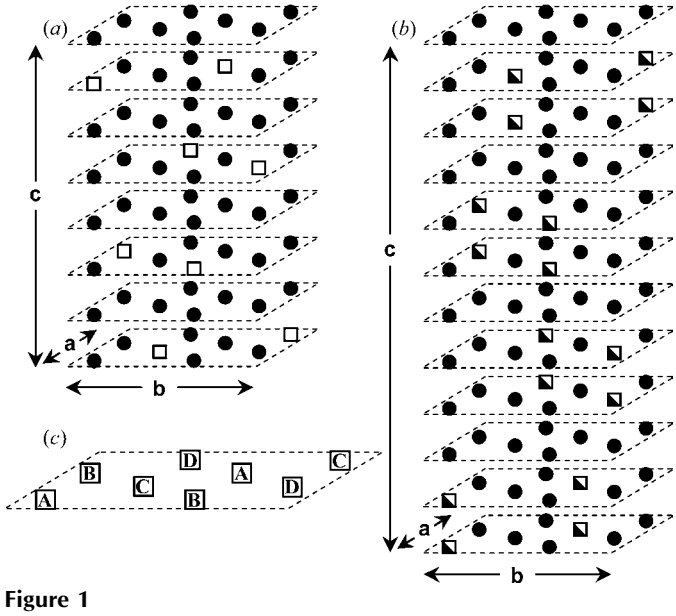

Figure 1
The superstructures for (*a*) the ideal 4*C*-type pyrrhotite (Fe_7S_8) proposed by Bertaut (1953) and (*b*) the 6*C*-type pyrrhotite ($Fe_{11}S_{12}$) described by Koto *et al.* (1975). Only the iron layers have been illustrated with sulfur layers omitted, where empty squares represent vacant sites and half-filled squares represent half an Fe atom. (*c*) Illustration of the nomenclature for vacant site positions (for the case of two vacancies in eight positions).

Intermediate (or non-integral) pyrrhotites (NC-type where $N = n/2$) are a metastable sub-group of low-temperature pyrrhotites with compositions that range between those of stable end-members 5*C* and 6*C*. They were shown not to persist in nature, exsolving to mixtures of Fe_9S_{10} with $Fe_{10}S_{11}$ or to $Fe_{10}S_{11}$ with $Fe_{11}S_{12}$ depending on the composition of the parent metastable phase (Morimoto *et al.*, 1975). The compositional difference between the stoichiometric end-members 5*C* and 6*C* is 0.57 wt % making it difficult to differentiate *NC* pyrrhotites directly based on compositional measurements (Morimoto *et al.*, 1975). From an electron-imaging study, Pierce & Buseck (1974) found that the 5*C* superstructure could be described by an ordered sequence of anti-phase domains, and that the *NC* superstructure could be described by a disordered sequence of anti-phase domains. Yamamoto & Nakazawa (1982) put forward a four-dimensional modulated structure model for pyrrhotite to describe all NC-type pyrrhotites. This model was refined to solve a 5.5*C* structure, which when extrapolated to 6*C* matched the superstructure vacancy distribution determined by Koto *et al.* (1975). Yamamoto & Nakazawa (1982) also extrapolated their model to make a prediction for the 5*C* structure, which contained an uneven distribution of vacancies with no full iron layers, a model presented only graphically making it difficult to verify. Yamamoto & Nakazawa's model was revised by Izaola *et al.* (2007). Izaola's revised model featured fully ordered vacancy distributions, where layers consisting of fully occupied iron layers combined with layers containing six in every eight iron sites occupied to form blocks which are separated by 'faults'. Kuban (1985) put forward an order–disorder structure interpretation for the whole family of pyrrhotites (Fe_7S_8 to FeS) using a family of order–disorder structural units which contained fully occupied iron layers and $\frac{3}{4}$ occupied iron layers.

Kruse (1990) conducted Mössbauer spectroscopy on a series of homogeneous synthetic pyrrhotites with *x* ranging from 0.004 to 0.143. Kruse found that the spectra from pyrrhotites whose compositions approach that of 4*C* could be described by three sextets associated with 0, 1 and 2 vacancies in the eight nearest neighbours adjacent to an iron atom. Likewise structures whose compositions approach that of 6*C* from the low vacancy side produce spectra which do not contain the sextet associated with 2 vacancies in 8, as they occur in 4*C*; instead they contained a sextet whose underlying source is unknown. Likewise a Mössbauer study by Schwarz & Vaughan (1972) revealed that pyrrhotites with *x* ranging between 0.113 and 0.148 produced spectra which are 4*C*-like and significantly different from the increasingly overlapping sextets of pyrrhotites with *x* ranging from 0.1 to 0. These observations are in accordance with the concept of vacancy repulsion or avoidance as described by Ward (1971) and Powell (1983) for pyrrhotites.

The vacancy distribution which occurs should vacancies be allowed to distribute across adjacent iron layers is an alternative interpretation of Koto's disordered statistical structure for 6*C*. Namely instead of layers containing two vacancies in eight adjacent to fully occupied iron layers, there are two layers both with one vacancy in eight. This interpretation appears to be in closer accordance with vacancy avoidance than the conventional stacking of full layers with $\frac{1}{4}$ vacant iron layers as in Nakazawa & Morimoto's proposed stacking sequence for 6*C*, Izaola's revised modulated structure model, or Kuban's order–disorder structure model, and is consistent with Mössbauer observations. In the present paper, a statistical structure model for pyrrhotite 5*C* has been put forward, which is analysed in the context of vacancy avoidance and ordering, and compared with the structure proposed by de Villiers *et al.* (2009).

There also appears to be some ongoing confusion in the literature with respect to the symmetry of the intermediate pyrrhotites. Carpenter & Desborough (1964) and Fleet & Macrae (1969), on their discovery classified pyrrhotites 5*C* and 6*C* as hexagonal. Vorma (1970) described 11*C* as apparently orthorhombic on its discovery, while Morimoto *et al.* (1970) simultaneously classified 11*C* as orthorhombic and suggested that the 5- and 6*C* pyrrhotites classified as hexagonal may potentially also be orthorhombic. Morimoto *et al.* (1970) put forward twinning with a 60 or 120° rotation about the pseudo-hexagonal *c* axis as the reason for apparent hexagonal symmetry. Koto *et al.* (1974) showed that 6*C* was monoclinic with pseudo-orthorhombic symmetry and partially ordered vacancies, which Morimoto, Gyobu, Mukaiyama & Izawa (1975) interpreted as suggesting that all NC pyrrhotites, including 5*C* and 6*C*, may be structurally monoclinic with partially ordered iron vacancies. Koto *et al.* (1975) described 6*C* as almost hexagonal with orthorhombic deformation observed at 130° 2θ with Fe $K\alpha$ radiation, and determined that 6*C* was in fact structurally monoclinic. Morimoto, Gyobu, Mukaiyama & Izawa (1975) described the NC pyrrhotites as apparently orthorhombic except 6*C* which is metrically orthorhombic but actually monoclinic, while still obtaining cell dimensions for 5-, 5.5- and 6*C* pyrrhotites on the assumption of hexagonal symmetry. Yamamoto & Nakazawa (1982) stated that an orthorhombic description of pyrrhotite structure for the NC pyrrhotites has been well established, while Wang & Salveson (2005) simply classified all NC pyrrhotites including the stable 5*C* and 6*C* end-members as hexagonal pyrrhotite. The symmetry of pyrrhotite 5*C* is considered in the context of this discourse.

2. Materials and methods

The pyrrhotite used in this study originated from the Renison Bell tin mine in Tasmania. Pyrrhotite from this locality has previously been described as containing a mixture of pyrrhotite 4*C* and 5*C* intergrowths (Haynes & Hill, 1970). The sample studied was selected from a collection of tablets sliced from cores drilled out of massive rock so as to contain a minimum of impurities. The tablet was milled in a Spex Certiprep 8000 mixer/mill (Ball Mill) for 2 min, with powder collected and unground pebble re-milled until sufficient powder was collected. The milled powder was then micronized with ethanol in a McCrone micronizing mill with agate grinding elements for 15 min, the suspended fines were decanted and the coarse fraction re-micronized until the whole sample was decanted, producing a fine powder which was used in this experiment. The ethanol was pan evaporated under ambient conditions for 2 d. The micronized pyrrhotite powder was mixed with SRM 640b silicon standard to roughly 5 wt % silicon and tapped into a 0.5 mm diameter glass capillary (Glas Technik & Konstruktion), which was sealed with candle wax.

Diffraction patterns were collected using the powder diffraction beamline at The Australian Synchrotron (Wallwork *et al.*, 2007) using 15.02 keV radiation with a 181 mA beam current for the pyrrhotite sample and 164 mA beam current for a lanthanum hexaboride standard, and the MYTHEN microstrip detector (Schmitt *et al.*, 2003) with a controlled hutch temperature of 299 ± 0.5 K. The detector contains over 20 400 channels with an average spacing of 0.00376° 2θ between each channel, excluding dead channels and 0.2° 2θ gaps between the 15, $\sim 5°$ 2θ modules. To compensate for the gaps in data, two diffraction patterns, each with a 300 s acquisition time, were collected offset by 0.5° 2θ for a combined 2θ ranging between 5 and 85°. The LaB_6 diffraction pattern was collected with a single acquisition of 30 s.

The diffraction patterns were analysed using Rietveld structure refinement (Rietveld, 1969) and quantitative Rietveld analysis (Hill & Howard, 1987) methods, with convolution-based profile fitting (Kern *et al.*, 2004) of the instrument profile using Bruker AXS TOPAS R3 software (Bruker AXS, 2005). The wavelength, refined to 0.825218 (1) Å, and instrument profile were refined using the National Institute of Standards (NIST) SRM 660a lanthanum hexaboride standard reference material (Freiman & Trahey, 2000), in conjunction with the instrument zero offset and a cylindrical 2θ correction. The structure determined by Straumanis & Aka (1952) was used to model the silicon internal standard in conjunction with the corrected lattice parameters for SRM 640b determined by Yoder-Short (1993). The presence of 4*C* and 5*C* structures was confirmed using the X-ray powder intensity data (powder diffraction files 29-0723 and 29-0724) indexed by Morimoto, Gyobu, Mukaiyama & Izawa (1975). The structure of 4*C* was modelled using the structure refined by Powell *et al.* (2004). Several trace phases which were found to be present in the sample were modelled so that their diffraction patterns would not interfere with the refinement of 5*C*, namely, arsenopyrite (Morimoto & Clark, 1961), cassiterite (Seki *et al.*, 1984), chalcopyrite (Hall & Stewart, 1973), fluorapatite (Sänger & Huhs, 1992), foitite (MacDonald *et al.*, 1993) and siderite (Effenberger *et al.*, 1981). The normalized composition was found to be 65.1 (6) wt% pyrrhotite 5*C* and 30.3 (5) wt% pyrrhotite 4*C* with foitite 2.1 (1) wt%, fluorapatite 1.38 (6) wt%, arsenopyrite 0.28 (2) wt%, siderite

Table 1
Coordinates of the 80 atom sites in the hexagonal unit cell of pyrrhotite 5*C*, for i and j = 1–10.

	x	y	z
Fe (i)	0	0	$0.1(i-1)$
Fe (10 + i)	0	0.5	$0.1(i-1)$
Fe (20 + i)	0.5	0	$0.1(i-1)$
Fe (30 + i)	0.5	0.5	$0.1(i-1)$
S (j)	2/3 (for odd j) 1/3 (for even j)	1/3 (for odd j) 2/3 (for even j)	$0.1(j-1)+0.05$
S (10 + j)	2/3 (for odd j) 5/6 (for even j)	5/6 (for odd j) 2/3 (for even j)	$0.1(j-1)+0.05$
S (20 + j)	1/6 (for odd j) 5/6 (for even j)	5/6 (for odd j) 1/6 (for even j)	$0.1(j-1)+0.05$
S (30 + j)	1/6 (for odd j) 1/3 (for even j)	1/3 (for odd j) 1/6 (for even j)	$0.1(j-1)+0.05$

0.44 (2) wt%, cassiterite 0.22 (1) wt% and chalcopyrite 0.19 (1) wt%.

3. Structure determination and refinement

The ideal NiAs structure was used to fill two structure models, one based on the hexagonal unit cell a = 6.88 and c = 28.7 Å described by Carpenter & Desborough (1964), the other based on the orthorhombic unit cell a = 6.8848, b = 11.936 and c = 28.6760 Å described by Morimoto *et al.* (1975). The unit-cell structures were built in the triclinic space group $P1$, and are detailed in Tables 1 and 2 (in compressed form) where there are ten layers of Fe atoms (i = 1 to 10) and ten layers of S atoms (j = 1 to 10) along the c axis. These tables can be expanded by substituting all values of i and j from 1 to 10. Mössbauer studies by Levinson & Treves (1968) and Vaughan & Ridout (1970) found no evidence for the presence of Fe^{3+} in pyrrhotite 4*C* and concluded that the iron sites in pyrrhotite could be sharing the charge, therefore, with a valency of +2.29. Based on a soft X-ray emission and Auger electron spectroscopic study, Marusak & Tongson (1979) found that all iron was present in the +2 state with the sulfide sublattice inhibiting the existence of Fe^{3+} through the donation of electrons. Therefore, the oxidation state of all Fe atoms was set to +2 to describe the X-ray scattering.

To begin the refinement, the silicon internal standard was used to determine the zero error and cylindrical 2θ correction, and all the known structure models for major and trace phases modelled with unit cell, crystallite size and strains refined. The 5*C* structure was initially modelled assuming all iron sites are 90% occupied, with isotropic displacement coefficients (B_{eq}) of 1 for all iron and sulfur sites. It was found that both the 4*C* and 5*C* pyrrhotite phases were bimodal in their crystallinity, which was modelled using two structure models each of which differed only in their unit cell, crystallite size and strains.

A comparison of fits to experimental data between the hexagonal and orthorhombic 5*C* structure models reveals that there is orthorhombic deformation of the underlying NiAs structure, analogous to the report by Koto *et al.* (1975) for 6*C*. It is evident at a d spacing of $\sim$ 1.016 where the single hexagonal peak has separated into a triplet of orthorhombic peaks which better model the multi-crested experimental data,

Table 2
Coordinates of the 160 atom sites in the orthorhombic unit cell of pyrrhotite 5*C*, for i and j = 1–10.

	x	y	z
Fe (i)	0	0	$0.1(i-1)$
Fe (10 + i)	0	0.5	$0.1(i-1)$
Fe (20 + i)	0.5	0	$0.1(i-1)$
Fe (30 + i)	0.5	0.5	$0.1(i-1)$
Fe (40 + i)	0.25	0.25	$0.1(i-1)$
Fe (50 + i)	0.25	0.75	$0.1(i-1)$
Fe (60 + i)	0.75	0.25	$0.1(i-1)$
Fe (70 + i)	0.75	0.75	$0.1(i-1)$
S (j)	0	1/6 (for odd j) 1/3 (for even j)	$0.1(j-1)+0.05$
S (10 + j)	0	2/3 (for odd j) 5/6 (for even j)	$0.1(j-1)+0.05$
S (20 + j)	0.5	1/6 (for odd j) 1/3 (for even j)	$0.1(j-1)+0.05$
S (30 + j)	0.5	2/3 (for odd j) 5/6 (for even j)	$0.1(j-1)+0.05$
S (40 + j)	0.25	5/12 (for odd j) 1/12 (for even j)	$0.1(j-1)+0.05$
S (50 + j)	0.25	11/12 (for odd j) 7/12 (for even j)	$0.1(j-1)+0.05$
S (60 + j)	0.75	5/12 (for odd j) 1/12 (for even j)	$0.1(j-1)+0.05$
S (70 + j)	0.75	11/12 (for odd j) 7/12 (for even j)	$0.1(j-1)+0.05$

discounting the hexagonal description. Pyrrhotite generally forms at high temperature with a random vacancy distribution and hexagonal symmetry. With cooling the unit-cell contracts and the vacancies start to order (Wang & Salveson, 2005). The orthorhombic symmetry expressed by the low-temperature pyrrhotites 5*C* and 6*C* suggest that this contraction is not uniform in each direction, being greater in the hexagonal direction $\mathbf{a}_1$ than in $\mathbf{a}_2$ and $\mathbf{a}_3$. At this point the key unknown is how the vacancies are arranged across the known NiAs base structure to form the superstructure of pyrrhotite 5*C*.

Faulting in the structure of pyrrhotite can break the repeating sequence of vacancies while leaving the underlying NiAs structure unaltered resulting in an asymmetry between vacancy reflection peaks and the main NiAs peaks. Given the significant strain in microstructure and the presence of major 4*C*-type pyrrhotite peaks overlapping with major 5*C*-type pyrrhotite peaks, no attempt was made to refine atomic positions away from their ideal values. Likewise all attempts to refine Fe occupancies resulted in substantial uncertainty and correlation between vacancies, and were therefore not pursued. Instead, a strategy of testing various postulated models against the powder diffraction data was employed. Fits were judged qualitatively based on the relative ratios of superstructure reflections in addition to the presence and absences of superstructure reflections.

Despite their inconsistency with Mössbauer observations, for the sake of the scientific method the vacancy distributions proposed by Corlett (1968) and Vaughan *et al.* (1971) were tested by setting the iron occupancies to 0 for vacant sites as indicated by Fig. 2, where i corresponds to the iron layer, with all other occupancies set to 1. As was the case for 6*C* (Koto *et al.*, 1975) these completely ordered vacancy models were unsuccessful at modelling the diffraction pattern, producing

significant discrepancies between observed and calculated superstructure reflections.

Koto *et al.* (1975) explained that their statistical structure model could be interpreted in terms of Nakazawa and Morimoto's occupancy distribution (*FAFFBFFCFFDF*) by employing a single iron layer out of step (*FFAFFBFFCFFD* + *FAFFBFFCFFDF*). Applying the same principle to the 5*C* vacancy distributions proposed by Corlett (1968) and Vaughan *et al.* (1971) gives the statistical structures $FA_{\frac{1}{2}}A_{\frac{1}{2}}B_{\frac{1}{2}}B_{\frac{1}{2}}C_{\frac{1}{2}}C_{\frac{1}{2}}D_{\frac{1}{2}}D_{\frac{1}{2}}F$ and $FA_{\frac{1}{2}}A_{\frac{1}{2}}B_{\frac{1}{2}}B_{\frac{1}{2}}FC_{\frac{1}{2}}C_{\frac{1}{2}}D_{\frac{1}{2}}D_{\frac{1}{2}}$. These statistical models for pyrrhotite 5*C* were tested using the ideal orthorhombic structure (Table 2) and $\frac{1}{2}$ iron occupancies for sites as indicated in Fig. 2, and found to provide equivalent fits to the diffraction data. Likewise, it was found that the crystallographically different vacancy layer sequences (1) $FA_{\frac{1}{2}}A_{\frac{1}{2}}B_{\frac{1}{2}}B_{\frac{1}{2}}FC_{\frac{1}{2}}C_{\frac{1}{2}}D_{\frac{1}{2}}D_{\frac{1}{2}}$ and (2) $FA_{\frac{1}{2}}A_{\frac{1}{2}}C_{\frac{1}{2}}C_{\frac{1}{2}}FB_{\frac{1}{2}}B_{\frac{1}{2}}D_{\frac{1}{2}}D_{\frac{1}{2}}$, both provided equivalent fits to the data and cannot be distinguished using powder diffraction.

With vacancy avoidance in mind and assuming the distribution of vacancies across layers is allowed (*e.g.* $FA_{\frac{1}{2}}A_{\frac{1}{2}}$ = FA^1A^2 and FA^2A^1 superimposed), the statistical pyrrhotite 5*C* models can be tested against the closeness condition. The site-to-site distance between A^1 and A^2 in the same iron layer is 6.89 Å, while between adjacent iron layers it is 7.46 Å. Any vacancy site arrangement that contains two vacancies with a separation significantly less than 6.89 Å must be forbidden; this is the closeness condition. For example, if the vacancies were distributed across all iron layers in 4*C* with one vacancy per layer (group of eight iron sites), there would be vacancy–vacancy separations of $\sim$ 4.5 Å which is forbidden. Instead 4*C* contains layers of two vacancies in a group of eight iron sites separated by layers fully occupied with iron and a minimum vacancy separation of 6.63 Å. Therefore, the sequence $FA_{\frac{1}{2}}A_{\frac{1}{2}}C_{\frac{1}{2}}C_{\frac{1}{2}}FB_{\frac{1}{2}}B_{\frac{1}{2}}D_{\frac{1}{2}}D_{\frac{1}{2}}$ is forbidden on account of a short 4.48 Å vacancy separation between some sites in adjacent iron layers, for example between A^2 and C^1 as well as B^2 and D^1 vacancy sites in adjacent iron layers for the stacking sequence $FA^1A^2C^1C^2FB^1B^2D^1D^2$. Likewise any model built with accumulated full iron layers will have vacancies with 4.48 Å separation, for example between B^2 and C^1 for the stacking sequence $FA^1A^2B^1B^2C^1C^2D^1D^2$F. Therefore, assuming:

(i) that vacancies distribute across adjacent iron layers in iron site parings as illustrated in Fig. 2, and

(ii) that all of the iron site positions host vacancies in a ten-iron layer 5*C* sequence,

then the sequence $FA_{\frac{1}{2}}A_{\frac{1}{2}}B_{\frac{1}{2}}B_{\frac{1}{2}}FC_{\frac{1}{2}}C_{\frac{1}{2}}D_{\frac{1}{2}}D_{\frac{1}{2}}$ and the crystallographically equivalent, structurally different, sequence $FA_{\frac{1}{2}}A_{\frac{1}{2}}B_{\frac{1}{2}}B_{\frac{1}{2}}FD_{\frac{1}{2}}D_{\frac{1}{2}}C_{\frac{1}{2}}C_{\frac{1}{2}}$ (chiral enantiomers) remain as the only viable solutions. For simplicity the discussion will focus on the sequence $FA_{\frac{1}{2}}A_{\frac{1}{2}}B_{\frac{1}{2}}B_{\frac{1}{2}}FC_{\frac{1}{2}}C_{\frac{1}{2}}D_{\frac{1}{2}}D_{\frac{1}{2}}$.

For independent verification, kinematic electron-diffraction patterns were calculated for the sequence $FA_{\frac{1}{2}}A_{\frac{1}{2}}B_{\frac{1}{2}}B_{\frac{1}{2}}FC_{\frac{1}{2}}C_{\frac{1}{2}}D_{\frac{1}{2}}D_{\frac{1}{2}}$ built in the hexagonal unit cell for comparison with the experimental 5*C* patterns published by Dódony & Pósfai (1990). The calculated patterns (see Fig. 3) closely match those of Dóndony & Pósfai adding weight to the validity of the structural solution.

The statistical structure for pyrrhotite 5*C* could be interpreted as an order–disorder structure. Starting with a vacancy in the iron-site position A^1, the only viable vacancy sequence to start with is $FA^1A^2B^1B^2$, which features a 6.62 Å vacancy separation between A^2 and B^1. In order to satisfy the average cell structure $FA_{\frac{1}{2}}A_{\frac{1}{2}}B_{\frac{1}{2}}B_{\frac{1}{2}}FC_{\frac{1}{2}}C_{\frac{1}{2}}D_{\frac{1}{2}}D_{\frac{1}{2}}$ determined previously, the starting sequence $FA^1A^2B^1B^2$ can only be followed by one of two possibilities, $FC^1C^2D^1D^2$ and $FC^2C^1D^2D^1$, which have a 6.69 Å vacancy separation between B^2FC^1 and between B^2FC^2. Likewise $FC^1C^2D^1D^2$ and $FC^2C^1D^2D^1$ can only be followed by either $FA^1A^2B^1B^2$ or $FA^2A^1B^2B^1$. These four vacancy sequences ($FA^1A^2B^1B^2$, $FA^2A^1B^2B^1$, $FC^1C^2D^1D^2$ and $FC^2C^1D^2D^1$) represent a set of translatable layers which can all be produced from a common structural unit through translation in the hexagonal $\mathbf{a}_2$-axis direction in steps of $\pm\mathbf{a}_2/2$ (3.44 Å) parallel to the hexagonal 001 plane. Dódony & Pósfai (1990) measured a 14.2 Å repeat distance in the hexagonal *c*-axis direction which is consistent with the structural unit. A rotation by 60 or 120° around the *c* axis and translations in multiple hexagonal axis directions cannot be occurring as superstructure building operations, since they would not generate the average cell structure. However, a rotation or

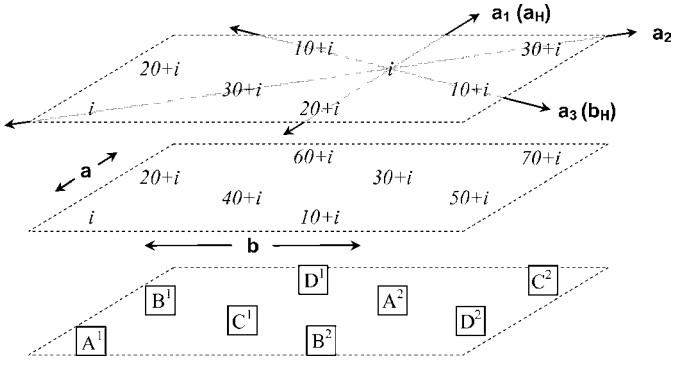

Figure 2
Relationship between vacancy nomenclature and iron-site positions for hexagonal and orthorhombic unit cells of pyrrhotite 5*C* (for the case of one vacancy in eight positions).

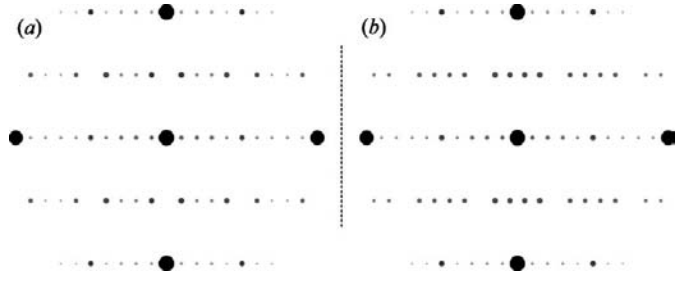

Figure 3
Kinematic electron-diffraction patterns for the hexagonal pyrrhotite 5*C* sequence $FA_{\frac{1}{2}}A_{\frac{1}{2}}B_{\frac{1}{2}}B_{\frac{1}{2}}FC_{\frac{1}{2}}C_{\frac{1}{2}}D_{\frac{1}{2}}D_{\frac{1}{2}}$ for zone axes (*a*) [1$\bar{1}$0] and (*b*) [210], simulated using JEMS at 100 kV, where the size of spots is indicative of the spot intensity.

Table 3
Atomic parameters for the 20 atom sites in the monoclinic unit cell of pyrrhotite $5Ca_3$, for k = 1–10.

	x	y	z	B_{eq}
Fe (k)	0.25	$0.1(k-1)$	0.25	1.87 (1)
S (k)	11/12 (for odd k) 7/12 (for even k)	$0.1(k-1)+0.05$	7/12 (for odd k) 11/12 (for even k)	0.70 (1)

change in the glide direction may still occur as faulting mechanisms.

The vacancies in the third and fourth iron layers of the structural unit are the closest of the vacancies in the resulting order–disorder structures, separated by 6.62 Å based on ideal atom-site positions, slightly less than the 6.63 Å separation between closest vacancies within the iron layers of pyrrhotite 4*C* (Powell *et al.*, 2004). It is hypothesized that repulsive forces between these voids may be a significant driving force behind the observed orthorhombic deformation. A shift of these vacancies slightly away from their ideal positions in the *c*-axis direction would further increase their separation. The alternatives of:

(i) a partial distribution of vacancies across layers (*e.g.* the starting sequences $FAFB^1B^2$, $FAFB^2B^1$, FA^1A^2FB and FA^2A^1FB), and

(ii) no distribution of vacancies across layers (*e.g.* the starting sequences *FAFBF*, *FAFFB* and *FFAFB*),

contain vacancies with a minimum separation of 6.69 Å based on ideal atom-site positions. They also contain a more disparate distribution of vacancies, which is inconsistent with the concept of vacancy repulsion and the significant change in the Mössbauer spectra, and therefore vacancy arrangement around Fe atoms, which occurs at 5*C* as observed by Schwarz & Vaughan (1972) and Kruse (1990) is decisive in its differentiation of a full distribution of vacancies across adjacent layers from the less distributed alternatives.

At this point it is worth applying the same tests to the 5*C* model of de Villiers *et al.* (2009). In that model, half of the vacancies are accumulated within two layers each containing two vacancies in every eight positions which is inconsistent with the combined Mössbauer findings of Vaughan *et al.* (1971) and Kruse (1990). Above and below these high vacancy layers are partially vacated layers which together contain 14% of the total vacancies, each of which is separated from vacancies in the high vacancy layers by less than 3 Å, a significant violation of the closeness condition. For these reasons the 5*C* structure proposed by de Villiers *et al.* (2009) is ruled out by the present approach.

A superstructure built from the *alternate gliding* of the structural unit in the hexagonal $\mathbf{a}_2$-axis direction is unable to explain the average cell structure of pyrrhotite 5*C*, producing significant discrepancies between observed and calculated superstructure reflections. A superstructure built through *echelon gliding* of the structural unit in the hexagonal $\mathbf{a}_2$-axis direction can explain the average cell structure of pyrrhotite 5*C*. However, it also produces significant discrepancies between observed and calculated superstructure reflections. Likewise, a building operation which involves the alternation of four positive glides along the hexagonal $\mathbf{a}_2$ axis followed by four negative glides could not model the observed superstructure reflections. Therefore, the layered structure must either have a complex long-range order or be disordered. A common feature of increasingly larger ordered superstructures like those tested is their associated increasing abundance of significant superstructure reflections, in stark contrast to the few which are experimentally observed, which is suggestive of a disordered or random stacking sequence of layers.

For simplicity the sulfur layers have previously been excluded from the discussion. The alternate stacking of sulfur in pyrrhotite results in two different structural units for pyrrhotite 5*C*, starting from A^1 they are $F\beta A^1\gamma A^2\beta B^1\gamma B^2\beta$ ($^{\beta}5^{\beta}$) and $F\gamma A^1\beta A^2\gamma B^1\beta B^2\gamma$ ($^{\gamma}5^{\gamma}$), where β and γ represent the two alternate sulfur layer configurations. Pyrrhotite 5*C* must be built using both structural units where a $^{\beta}5^{\beta}$ unit is always preceded and followed by a $^{\gamma}5^{\gamma}$ unit and *vice versa*. Likewise the obvious extension of this order–disorder model is to pyrrhotite 6*C*, for which the structural units starting from A^1 are $F\beta A^1\gamma A^2\beta F\gamma B^1\beta B^2\gamma$ ($^{\beta}6^{\gamma}$) and $F\gamma A^1\beta A^2\gamma F\beta B^1\gamma B^2\beta$ ($^{\gamma}6^{\beta}$). Pyrrhotite 6*C* must be built using only one of these units. An order–disorder structural model could be employed to describe pyrrhotite 11*C* and all the other intermediate pyrrhotites between 5*C* and 6*C* using the four building units $^{\beta}5^{\beta}$, $^{\gamma}5^{\gamma}$, $^{\beta}6^{\gamma}$ and $^{\gamma}6^{\beta}$, where the intermediate pyrrhotites together form a polysomatic series. For stoichiometry, pyrrhotite 11*C* would be built from an equal quantity of 5*C* and 6*C* structural units. For consistency with vacancy avoidance, each 5*C* unit would be followed by a 6*C* unit and *vice versa*, such that the repeating sequence of units would be $[^{\beta}5^{\beta}\text{–}^{\gamma}6^{\beta}\text{–}^{\gamma}5^{\gamma}\text{–}^{\beta}6^{\gamma}]$, where each individual structural unit is offset from adjacent units by a glide of $\pm a_2/2$ (or $\pm a_3/2$) in the hexagonal axis direction.

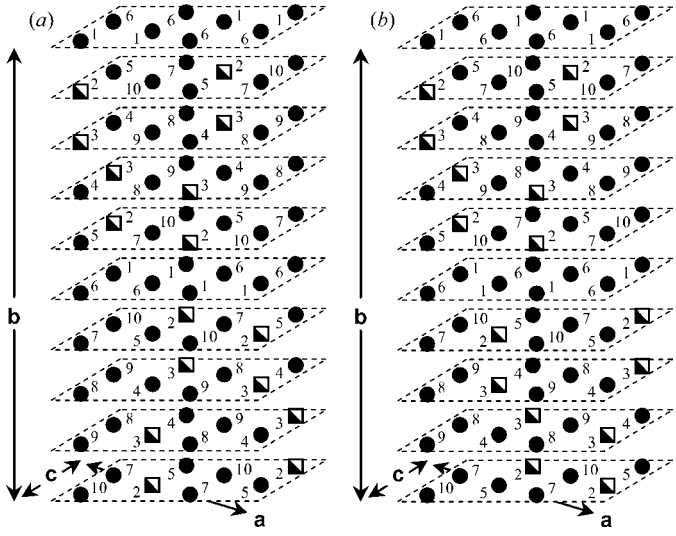

Figure 4
Superstructure solution for monoclinic pyrrhotite 5*C* (Fe_9S_{10}) enantiomers (*a*) $5Ca_3$, and (*b*) $5Ca_2$, with iron site positions numbered. Only the iron layers have been illustrated with sulfur layers omitted, and half-filled squares represent half an Fe atom.

Table 4
Atomic parameters for the 20 atom sites in the monoclinic unit cell of pyrrhotite $5Ca_2$, for k = 1–10.

	x	y	z	B_{eq}
Fe (k)	0.25	$0.1(k-1)$	0	1.86 (1)
S (k)	11/12 (for odd k) 7/12 (for even k)	$0.1(k-1)+0.05$	1/3 (for odd k) 2/3 (for even k)	0.70 (1)

The ADDSYM feature in *PLATON* (Spek, 2003) was used to determine the highest crystallographic symmetry description of the statistical pyrrhotite 5*C* structure ($FA_{\frac{1}{2}}A_{\frac{1}{2}}B_{\frac{1}{2}}B_{\frac{1}{2}}FC_{\frac{1}{2}}C_{\frac{1}{2}}D_{\frac{1}{2}}D_{\frac{1}{2}}$), which was found to be provided by the monoclinic space group $P2_1/c$ with the ideal atom sites listed in Table 3, where Fe#2 and Fe#3 have half occupancies as illustrated in Fig. 4(*a*). The structure described in Table 3 has the statistical layer sequence $FA_{\frac{1}{2}}A_{\frac{1}{2}}B_{\frac{1}{2}}B_{\frac{1}{2}}FD_{\frac{1}{2}}D_{\frac{1}{2}}C_{\frac{1}{2}}C_{\frac{1}{2}}$ ($5Ca_3$), which is crystallographically equivalent to and structurally different from $FA_{\frac{1}{2}}A_{\frac{1}{2}}B_{\frac{1}{2}}B_{\frac{1}{2}}FC_{\frac{1}{2}}C_{\frac{1}{2}}D_{\frac{1}{2}}D_{\frac{1}{2}}$ ($5Ca_2$), which can also be described by the monoclinic space group $P2_1/c$ with the ideal atom sites listed in Table 4, where Fe#2 and Fe#3 have half occupancies as illustrated in Fig. 4(*b*). Although two alternative structures have been presented, it is beyond the scope of the present paper to demonstrate whether either $5Ca_2$ or $5Ca_3$, or both $5Ca_2$ and $5Ca_3$ occur in nature. The cell dimensions after refinement are summarized in Table 5[1] for $5Ca_2$. Owing to the statistical nature of the vacancy sites resulting from the superposition of two position states of the structural unit, there are two scenarios to consider. First where there is a vacancy in the site, neighbouring Fe and S atoms may be shifted slightly toward the vacancy position as is the case in 4*C* (Tokonami *et al.*, 1972). Alternatively, where there is an iron atom in the site the nearest neighbouring atoms would have positions relatively close to ideal. The averaging of two sets of Fe-atom positions in the average 'statistical' structure is reflected in the relatively high displacement coefficient for iron relative to sulfur.

There is an accurately measured range of uncertainty associated with both LaB_6 and silicon standards in addition to an uncertainty associated with the actual sample temperatures during analysis. Therefore, the final refinement of LaB_6 and pyrrhotite sample diffraction patterns were conducted simultaneously with all refined parameters open and with LaB_6 and silicon lattice parameters allowed to refine within ±3 deviations of reported standard error (including ±0.5°C for LaB_6) so that all known sources of uncertainty are reflected in the results. The silicon unit cell did not deviate from the reported average while the observed deviation in LaB_6 from its reported average is more likely a reflection of its actual measurement temperature than a deviation from its reported lattice parameter. The refinement figures of merit are summarized in Table 5 for the $5Ca_3$ phase. The experimental, model and difference curves are presented in Fig. 5, where the small offsets in some of the minor superstructure reflection

Table 5
Crystal data and refinement details using pyrrhotite $5Ca_3$.

For all structures: Fe_9S_{10}, M_r = 823.26, monoclinic, $P2_1/c$, Z = 4. Experiments were carried out at 299 K with synchrotron radiation, λ = 0.825218 (1) Å using a MYTHEN microstrip detector diffractometer. Refinement was on 117 parameters with 76 restraints.

Crystal data	
a, b, c (Å)	6.89268 (16), 28.6721 (3), 6.88520 (8)
β (°)	119.956 (2)
V (Å^3)	1178.93 (4)
μ (mm^{-1})	18.91 (1)
Specimen shape, size (mm)	Cylinder, 70 × 0.5
Data collection	
Specimen mounting	Glass capillary
Data collection mode	Transmission
Scan method	Stationary detector
Refinement	
R factors and goodness of fit	R_p = 0.024, R_{wp} = 0.034, R_{exp} = 0.012, R_{Bragg} = 0.020, χ^2 = 8.358
No. of data points	61 115

Computer programs used: *TOPAS* (Bruker AXS, 2005) and *PLATON* (Spek, 2003).

positions may be indicative of the reduction of larger superstructure to produce the average structure. Alternatively, the small offsets may be the result of uniform strain in the superstructure.

Although the underlying NiAs structure is orthorhombic, the arrangement of vacancies has resulted in a superstructure which has lower symmetry than that of the underlying NiAs structure, best described by a monoclinic space group. Therefore, pyrrhotite 5*C* can be described as monoclinic or pseudo-orthorhombic as is the case for pyrrhotite 6*C*.

By combining the results of Kruse (1990) and Schwarz & Vaughan (1972) it can be seen that the Mössbauer sextets associated with two vacancies in eight, as they occur in pyrrhotite 4*C*, are not present in the pyrrhotites with x ranging from 0.1 to 0. In its place a new sextet with an unknown underlying source was present. In the absence of a structural description, Kruse (1990) speculated that there may be an effect by vacancies beyond the eight nearest iron positions. From a comparison of the presented 5*C* structure with that of 4*C*, the differences require consideration of vacancies surrounding the neighbouring Fe atoms. The key distinguishing feature is that pyrrhotite 4*C* contains iron layers with two vacancies in every eight site positions such that each Fe atom has two neighbouring vacancies and four neighbouring planar Fe atoms, each of which has two neighbouring vacancies. In contrast, 5*C* also contains some iron atoms with two neighbouring vacancies; however, the four neighbouring planar Fe atoms each contain only one neighbouring vacancy. The presence of increased vacancies surrounding the nearest planar Fe atoms in 4*C* enhances the contraction in the hyperfine field relative to the 5*C* case, confirming Kruse's postulation, and indicating increased covalency in the case of 4*C* relative to 5*C*, consistent with the measurements of Marusak & Tongson (1979).

The 5*C* structure as presented is ideal in that the atom-site positions have not been refined from their ideal NiAs posi-

[1] Supplementary data for this paper are available from the IUCr electronic archives (Reference: KD5037). Services for accessing these data are described at the back of the journal.

tions. Such a refinement could be performed from a single-crystal diffraction experiment and would require that all the fully occupied atom-site positions be split into two half-occupied positions, each of which represent the two displaced positions of the structural unit which are superimposing when projected into the average structure. The two sets of half-occupied site positions can be related to each other by $\pm a_2$ or $\pm a_3$ (6.89 Å) for $5Ca_2$ and $5Ca_3$. The primary challenge is to obtain with verification a single crystal of stoichiometric 5*C*, which is complicated by the following properties that make this task formidable:

(i) A pyrrhotite crystal can in theory consist of multiple continuous domains in terms of superstructure while simultaneously containing a single continuous domain in terms of its base NiAs-type structure.

(ii) There are two special cases of the previous point to consider. First where there is a change in the structure-building glide direction in which case the crystallographically equivalent zone axes of the two structure domains, $5Ca_2$ and $5Ca_3$, are misaligned by rotation around the hexagonal *c* axis; the second special case occurs where there is a transition from one NC-type domain to another, *e.g.* 5*C* to 11*C*, with the hexagonal *c* axis common to both domains.

(iii) For pyrrhotites which have experienced high temperatures in their geological history, the transition from hexagonal to pseudo-orthorhombic which takes place during the transition to 5*C* is conducive to twinning (Buerger, 1945; Hahn & Klapper, 2006).

(iv) If the composition of high-temperature hexagonal parent pyrrhotite is between that of 4*C* and 5*C*, geological cooling to equilibrium will result in the exsolution of stoichiometric 4*C* and 5*C*, where the resulting mixture of 4*C* and 5*C* intergrowths are uncongenial to single-crystal isolation.

(v) Intergrowths of 4*C* with 5*C* can at least be visually observed through etching (Haynes & Hill, 1970). The analogous characterization of intergrowths of 5*C* with 11*C* has not been cited. In the absence of distinguishing features, intergrowths of 5*C* with 11*C* would be less congenial to single-crystal isolation than intergrowths of 4*C* with 5*C*.

An alternative approach to the study of pyrrhotite 5*C* in particular and NC pyrrhotites in general is computational analysis. Computational analysis offers the possibility of evaluating the deviation of atoms from their ideal site positions, the driving forces behind orthorhombic deformation, and the proposed OD model for NC polysomatic series. However, the complexity posed by the disordered nature of these structures puts this problem 'beyond what can be reliably achieved with present day methods' (Gale, 2010).

4. Conclusions

The structure of pyrrhotite 5*C* has been investigated by evaluating the viable distribution of vacancy sites across the known ideal NiAs base structure:

(i) subject to the assumption that spatially different vacancy layer configurations *A*, *B*, *C* and *D* demonstrated to occur in pyrrhotite 4*C* also occur in 5*C* in a form where vacancies distribute across adjacent iron layers; and

(ii) subject to constraints imposed by maximum vacancy separation (vacancy avoidance), the closeness condition, and Mössbauer observations drawn from Schwarz & Vaughan (1972) and Kruse (1990).

An order–disorder approach has been employed, where only two structural units ($^{\beta}5^{\beta}$ and $^{\gamma}5^{\gamma}$) could be built which do not violate the constraints. These structural units differ only in the symmetry of sulfur arrangement relative to iron. 5*C* superstructures are built from the alternate layering of $^{\beta}5^{\beta}$ and $^{\gamma}5^{\gamma}$ structure units with a glide in either the a_2 or a_3 hexagonal axis direction. The structure was shown to be disordered, where two crystallographically equivalent statistical solutions ($FA_{\frac{1}{2}}A_{\frac{1}{2}}B_{\frac{1}{2}}B_{\frac{1}{2}}FC_{\frac{1}{2}}C_{\frac{1}{2}}D_{\frac{1}{2}}D_{\frac{1}{2}}$ and $FA_{\frac{1}{2}}A_{\frac{1}{2}}B_{\frac{1}{2}}B_{\frac{1}{2}}FD_{\frac{1}{2}}D_{\frac{1}{2}}C_{\frac{1}{2}}C_{\frac{1}{2}}$) could be produced from the structural units, which differ in the superstructure

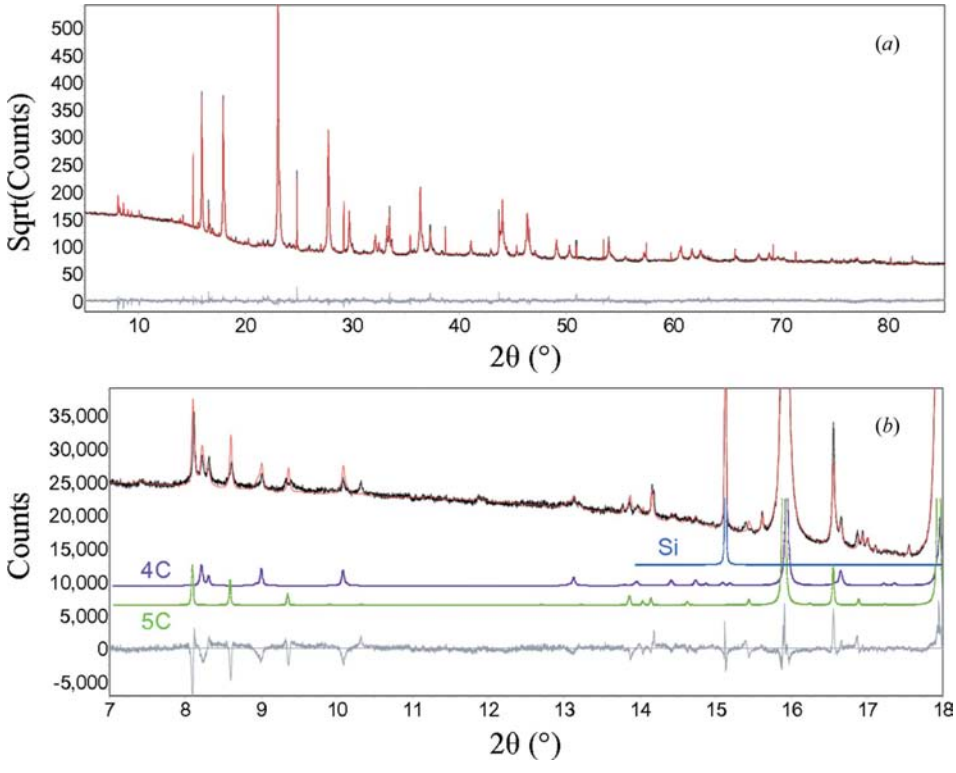

Figure 5
Experimental, model and difference curves for refinement over (*a*) the full range of 2θ, and (*b*) spanning the main superstructure reflections, generated using $5Ca_3$.

building glide direction (a_2 *versus* a_3). These structural solutions ($5Ca_2$ and $5Ca_3$) are consistent with both synchrotron powder diffraction data as well as the electron-diffraction patterns measured by Dódony & Pósfai (1990), adding weight to the validity of the structural solutions. The statistical structure for pyrrhotite 5*C* is best described by the monoclinic space group $P2_1/c$. An order–disorder structural model has been proposed for the intermediate pyrrhotites (5*C* to 6*C*) based on the regular sequencing of up to four structural units which are disordered through a glide in a single hexagonal axis direction ($\pm a_2/2$ or $\pm a_3/2$). Since both end-members of the intermediate pyrrhotites are pseudo-orthorhombic, the whole polysomatic series is likely to be pseudo-orthorhombic.

The interpretation presented by Kruse (1990) for Mössbauer sextets has been completed in the context of 5*C* structures determined, and significant challenges associated with improving the structural solution beyond the present ideal form were discussed.

The support of the CSIRO Minerals Down Under Flagship and Parker CRC for Integrated Hydrometallurgy Solutions (established and supported under the Australian Government's Cooperative Research Centres Program) is gratefully acknowledged. The author would like to thank Derek Winchester, CSIRO Earth Science and Resource Engineering, for preparing the pyrrhotite tablets, to thank Professor Martin Saunders, Centre for Microscopy, Characterization and Analysis at the University of Western Australia, for generating kinematic electron diffraction patterns in JEMS, and to gratefully acknowledge the assistance provided by Dr Kia Wallwork who collected the data on the Powder diffraction beamline at the Australian Synchrotron, Victoria, Australia.

References

Bertaut, E. F. (1953). *Acta Cryst.* **6**, 557–561.
Bertaut, E. F. (1956). *Bull. Soc. Fr. Miner. Crist.* **LXXIX**, 276–292.
Bruker AXS (2005). *TOPAS*, Version 3. Bruker AXS Inc., Karlsruhe, Germany.
Buerger, M. J. (1945). *Am. Mineral.* **30**, 469–482.
Carpenter, R. H. & Desborough, G. A. (1964). *Am. Mineral.* **49**, 1350–1365.
Corlett, M. (1968). *Z. Kristallogr.* **126**, 124–134.
Dódony, I. & Pósfai, M. (1990). *Eur. J. Mineral.* **2**, 529–535.
Effenberger, H., Mereiter, K. & Zemann, J. (1981). *Z. Kristallogr.* **156**, 233–243.
Evans, H. T. (1970). *Science*, **167**, 621–623.
Fleet, M. E. & Macrae, N. (1969). *Can. Mineral.* **9**, 699–705.
Freiman, S. W. & Trahey, N. M. (2000). *Standard Reference Material*® 660*a, Lanthanum Hexaboride Powder Line Position and Line Shape Standard for Powder Diffraction*, Certificate. National Institute of Standards and Technology.
Gale, J. (2010). Letter to A. D. Elliot, 22 January 2010. Nanochemistry Research Institute, Department of Chemistry, Curtin University of Technology.
Hahn, Th. & Klapper, H. (2006). *International Tables for Crystallography*, edited by A. Authier, pp. 393–448. Dordrecht: Kluwer Academic Publishers.
Hall, S. R. & Stewart, J. M. (1973). *Acta Cryst.* B**29**, 579–585.
Haynes, S. J. & Hill, P. A. (1970). *Econ. Geol.* **65**, 838–848.
Hill, R. J. & Howard, C. J. (1987). *J. Appl. Cryst.* **20**, 467–474.
Izaola, Z., González, S., Elcoro, L., Perez-Mato, J. M., Madariaga, G. & García, A. (2007). *Acta Cryst.* B**63**, 693–702.
Kern, A., Coelho, A. A. & Cheary, R. W. (2004). *Diffraction Analysis of the Microstructure of Materials*, edited by E. J. Mittemeijer & P. Scardi, pp. 17–50. New York: Springer.
Koto, K., Morimoto, N. & Gyobu, A. (1974). *Diffraction Studies of Real Atoms and Real Crystals: Abstracts of Papers Presented at the International Crystallography Conference held in Melbourne*, edited by T. J. Bastow, pp. 161–162. Melbourne, Australia: Australian Academy of Science.
Koto, K., Morimoto, N. & Gyobu, A. (1975). *Acta Cryst.* B**31**, 2759–2764.
Kruse, O. (1990). *Am. Mineral.* **75**, 755–763.
Kuban, R. J. (1985). *Cryst. Res. Technol.* **20**, 1649–1656.
Levinson, L. M. & Treves, D. (1968). *J. Phys. Chem. Solids*, **29**, 2227–2231.
MacDonald, D. J., Hawthorne, F. C. & Grice, J. D. (1993). *Am. Mineral.* **78**, 1299–1303.
Marusak, L. A. & Tongson, L. L. (1979). *J. Appl. Phys.* **50**, 4350–4355.
Morimoto, N. & Clark, L. A. (1961). *Am. Mineral.* **46**, 1448–1468.
Morimoto, N., Gyobu, A., Mukaiyama, H. & Izawa, E. (1975). *Econ. Geol.* **70**, 824–833.
Morimoto, N., Gyobu, A., Tsukuma, K. & Koto, K. (1975). *Am. Mineral.* **60**, 240–248.
Morimoto, N., Nakazawa, H., Nishiguchi, K. & Tokonami, M. (1970). *Science*, **168**, 964–966.
Nakazawa, H. & Morimoto, N. (1971). *Mater. Res. Bull.* **6**, 345–358.
Nakazawa, H., Morimoto, N. & Watanabe, E. (1975). *Am. Mineral.* **60**, 359–366.
Pierce, L. & Buseck, P. R. (1974). *Science*, **186**, 1209–1212.
Powell, A. V., Vaqueiro, P., Knight, K. S., Chapon, L. C. & Sánchez, R. D. (2004). *Phys. Rev. B Condens. Matter*, **70**, 014415(1–12).
Powell, R. (1983). *Mineral. Mag.* **47**, 437–440.
Rietveld, H. M. (1969). *J. Appl. Cryst.* **2**, 65–71.
Sänger, A. T. & Huhs, W. F. (1992). *Z. Kristallogr.* **199**, 123–148.
Schmitt, B., Brönnimann, Ch., Eikenberry, E. F., Gozzo, F., Hörmann, C., Horisberger, R. & Patterson, B. (2003). *Nucl. Instrum. Methods Phys. Res. A*, **501**, 267–272.
Schwarz, E. J. & Vaughan, D. J. (1972). *J. Geomag. Geoelectr.* **24**, 441–458.
Seki, H., Ishizawa, N., Mizutani, N. & Kato, M. (1984). *J. Ceram. Soc. Jpn*, **92**, 219–223.
Spek, A. L. (2003). *J. Appl. Cryst.* **36**, 7–13.
Straumanis, M. E. & Aka, E. Z. (1952). *J. Appl. Phys.* **23**, 330–334.
Tokonami, M., Nishiguchi, K. & Morimoto, N. (1972). *Am. Mineral.* **57**, 1066–1080.
Van Landuyt, J. & Amelinckx, S. (1972). *Mater. Res. Bull.* **7**, 71–80.
Vaughan, D. J. & Ridout, M. S. (1970). *Solid State Commun.* **8**, 2165–2167.
Vaughan, D. J., Schwarz, E. J. & Owens, D. R. (1971). *Econ. Geol.* **66**, 1131–1144.
Villiers, J. P. R. de & Liles, D. C. (2010). *Am. Mineral.* **95**, 148–152.
Villiers, J. R. R. de, Liles, D. C. & Becker, M. (2009). *Am. Mineral.* **94**, 1405–1410.
Vorma, A. (1970). *Bull. Geol. Soc. Finland*, **42**, 3–12.
Wallwork, K. S., Kennedy, B. J. & Wang, D. (2007). *Synchrotron Radiation Instrumentation: Ninth International Conference on Synchrotron Radiation Instrumentation*, edited by J. Y. Choi & S. Rah, pp. 879–882. Melville, New York: American Institute of Physics.
Wang, H. & Salveson, I. (2005). *Phase Transitions*, **78**, 547–567.
Ward, J. C. (1971). *Solid State Commun.* **9**, 357–359.
Yamamoto, A. & Nakazawa, H. (1982). *Acta Cryst.* A**38**, 79–86.
Yoder-Short, D. (1993). *J. Appl. Cryst.* **26**, 272–276.